Fano effect in an ultracold atom-molecule coupled system

Yuqing Li,[1,2] Guosheng Feng,[1] Jizhou Wu,[1,2] Jie Ma,[1,2,*] Bimalendu Deb,[3,4,†] Arpita Pal,[4] Liantuan Xiao,[1,2] and Suotang Jia[1,2]

[1]*State Key Laboratory of Quantum Optics and Quantum Optics Devices, Institute of Laser Spectroscopy, College of Physics and Electronics Engineering, Shanxi University, Taiyuan 030006, People's Republic of China*

[2]*Collaborative Innovation Center of Extreme Optics, Shanxi University, Taiyuan 030006, People's Republic of China*

[3]*Raman Centre for Atomic, Molecular and Optical Sciences, Indian Association for the Cultivation of Science, Jadavpur, Kolkata 700032, India*

[4]*Department of Materials Science, Indian Association for the Cultivation of Science, Jadavpur, Kolkata 700032, India*

(Received 29 September 2018; published 8 February 2019)

The Fano resonance, with a unique asymmetric line shape, is a well-known manifestation of quantum interference with numerous promising applications for light-harvesting devices. Here we report an experimental observation of the Fano effect in an ultracold atom-molecule coupled system realized by photoassociation near a magnetically tunable d-wave Feshbach resonance. Our result shows that, compared to ubiquitous single-peak Fano-type line shapes, the coupled Fano resonances feature a two-peak profile. We develop a theory of coupled Fano resonances which agrees very well with the experimental results. This work may open a new perspective for tuning ultracold collisional interaction using the Fano resonance and studying bound states in continuum.

DOI: 10.1103/PhysRevA.99.022702

I. INTRODUCTION

The dispersive and nontrivial line shapes exhibited by resonantly coupled physical systems are of high interest in many fields [1,2]. One paradigmatic example is represented by the Fano resonance [3,4], a ubiquitous phenomenon that has been observed in molecular spectroscopy [5] and in the fluorescence or absorption of diverse systems ranging from atomic [6,7] and nuclear [8,9] to solid-state systems [10,11]. Characterized by asymmetric line shapes, the Fano effect arises when quantum interference occurs between two competing optical paths: one connects a continuum of states to a discrete state, while the other couples a bound state embedded in the continuum to this discrete state. The unique properties associated with the Fano line shapes, particularly in optical nanoscale systems, such as semiconductors, quantum dots, and photonic crystals [12–14], are highly promising in many potential applications, including optical filtering [15], sensing [16], all-optical switching [17], and novel photonic devices.

In the above Fano resonances in individual systems, the coupling of a discrete state to a continuum of states through an autoionizing or analogous process is, in general, uncontrollable. Although intensive efforts toward precisely controlling asymmetric line shape have made significant progress, studies on the control of this pivotal coupling between the discrete state and continuum still have great interest. Recently, Fano resonances with tunable coupling between the discrete state and continuum were attained in the coupled plasmonic-molecular [18,19] and plasmonic-atomic [20] systems, in which the tunable broad plasmonic resonance is resonantly coupled to a narrow atomic or molecular resonance. It would therefore be of great interest to further explore such an effect in a coupled ultracold atomic-molecular system, where ultracold atoms and molecules can precisely be controlled experimentally. In particular, the magneto-optically tunable coupling between the atomic continuum and the molecular bound states promises to generate asymmetric Fano line shapes, which can be controlled by magnetically tuning the energy of a quasibound state [21] in the presence of optical continuum-bound and bound-bound couplings [22].

In this work, we report an experimental demonstration of the Fano resonances in an ultracold atom-molecule coupled system. We reveal the Fano effect in the spectra of atom loss as a function of the magnetic field tuned close to a d-wave quasibound state in the presence of photoassociation (PA) of ultracold Cs atoms. The continuum-bound PA transitions between the atomic collisional continuum and an excited molecular state are resonantly coupled to the bound-bound transitions between the quasibound state and the excited state. In the absence of a PA laser, the tunable magnetic field induces a multichannel scattering resonance (known as a magnetic Feshbach resonance) in the ground-state manifold. In fact, both Feshbach and Fano resonances describe a continuum-bound coupled system. However, by Fano effect we here refer to a physical situation where a continuum-bound superposition state is optically coupled to one or multiple bound states, leading to an asymmetric spectral profile. Our results feature, aside from the familiar Fano minimum reflecting the underlying destructive quantum interference, an intriguing two-peak structure. We explain these findings as a result of dual Fano resonances, and our theoretical model provides very good quantitative agreement with the experimental data.

II. THE EXPERIMENT

We prepare the ultracold ^{133}Cs atoms in the hyperfine state $F = 3, m_F = 3$ using three-dimensional degenerated Raman sideband cooling, after which the atoms are magnetically

*Corresponding author: mj@sxu.edu.cn
†Corresponding author: msbd@iacs.res.in

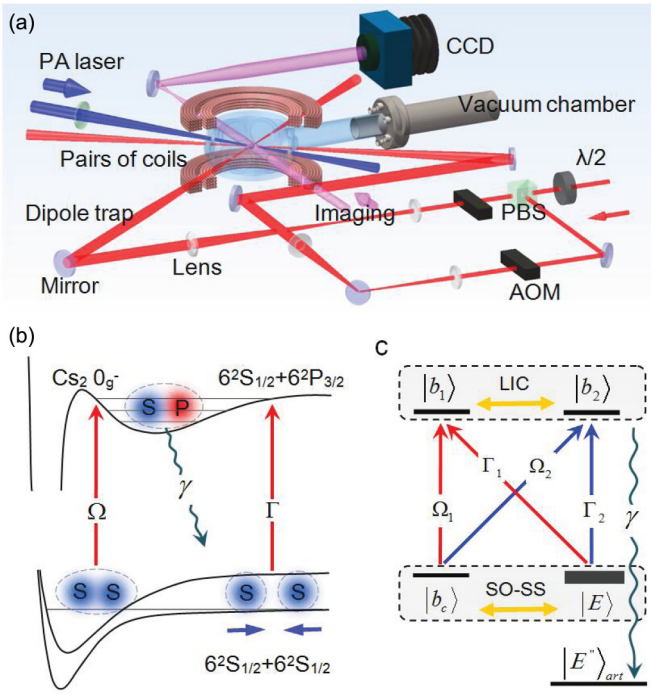

FIG. 1. Experimental details and schematic of energy levels and their couplings. (a) Experimental geometry and configuration of both lasers and magnetic coil pairs for generating Fano resonances. (b) A schematic diagram of molecular potential. A pair of Cs atoms in the open channel is coupled to a d-wave bound molecular state in the closed channel $|c\rangle$ via Feshbach resonance. The PA laser near resonant with the free-bound transition can also induce the bound-bound transition and forms electronically excited molecular bound states in the outer well of the 0_g^- potential below the $6S_{1/2} + 6P_{3/2}$ threshold. (c) Scheme for coupled dual Fano resonances. The same PA laser can induce couplings of both $|E\rangle$ and $|b_c\rangle$ to two quasidegenerate excited molecular states, $|b_1\rangle$ and $|b_2\rangle$, having the same vibrational and rotational quantum numbers but different molecular hyperfine quantum numbers.

levitated loaded into a crossed optical dipole trap [23]. The experimental setup for magnetically levitated loading the cooled atoms and generating the Fano resonance are shown in Fig. 1(a). The crossed dipole trap is formed by intersecting two 1064 nm laser beams in the horizontal directions; the dipole lasers are focused on the center of the vacuum chamber with $1/e^2$ beam radii of 230 and 240 μm. The outer pairs of magnetic field coils create the magnetic field gradient of $\partial B/\partial z = 31.3\,\mathrm{G/cm}$ in the center of the atomic sample for magnetically levitating the cooled atoms. Meanwhile the inner pairs of magnetic coils form a uniform magnetic field of $\sim$75 G in the z direction to cancel the resulting antitrapping potential in the horizontal direction from the application of the vertical magnetic field gradient. Then, an efficient thermal equilibrium process dominated by a strong three-body loss is implemented for 500 ms at a magnetic field of $B = 75$ G, corresponding to the scattering length $a = 1200a_0$ [24], with a_0 being the Bohr radius. The resulting atomic sample is measured to have 2.5×10^5 Cs atoms with a temperature of $T = 3.5\,\mu$K.

Next, the uniform magnetic field is adiabatically ramped down to the vicinity of the d-wave Feshbach resonance of ultracold Cs atoms [25]. Afterwards, we switch on a PA laser with an intensity of $I = 141.5\,\mathrm{W/cm^2}$ to illuminate the optically trapped atoms for 100 ms. Due to the efficient thermal equilibrium process dominated by the strong three-body loss whose rate is proportional to the third power of atom density, the dilute atomic sample in our experiment exhibits negligible atom loss as a response to the d-wave Feshbach resonance. Therefore, we can attribute the variation in the number of atoms remaining in the dipole trap to the PA-induced loss that is largely modified when the magnetic field is tuned near the d-wave Feshbach resonance.

III. RESULTS AND DISCUSSIONS

As illustrated in Fig. 1(b), in the presence of the d-wave Feshbach resonance described by a standard two-channel model [21], application of a single PA laser can cause both the continuum of atomic scattering states and quasibound state $|b_c\rangle$ embedded in the continuum to be simultaneously coupled to an excited molecular bound state. Specifically, when the laser is tuned near the resonance to a continuum-bound transition, a pair of colliding atoms in the continuum are photoassociated to form an excited molecule in their bound state, which is located in the outer well of the Cs_2 0_g^- potential [26] with the $6S_{1/2} + 6P_{3/2}$ asymptote. This gives rise to two competing optical pathways to an excited molecular bound state, i.e., continuum-bound and bound-bound PA transitions, so that their quantum interference leads to the Fano resonance. In general, a single PA laser can couple several excited bound molecular states because of the hyperfine splitting of the molecular rovibrational levels [27], resulting in multiple Fano profiles, as demonstrated previously in the context of nonlinear optical effects using multiple autoionizing [28]. Figure 1(c) shows a brief but relevant case involving two excited bound states, labeled $|b_1\rangle$ and $|b_2\rangle$. As is shown, two Fano resonances can arise, one from competing transitions from both $|E\rangle$ and $|b_c\rangle$ to $|b_1\rangle$ (red curves) and the other associated with couplings of $|E\rangle$ and $|b_c\rangle$ to $|b_2\rangle$ (blue curves). Both states $|b_1\rangle$ and $|b_2\rangle$ can spontaneously decay to a decay channel modeled as an artificial state $|E''\rangle_{\mathrm{art}}$ representing a PA loss [29]. These decay processes are correlated, rendering an observable manifestation of the coupled Fano resonances, as we show below.

We measure the atom loss and observe how it is affected by the magnetic field tuned close to a d-wave quasibound state. In Fig. 2, we present our results for the laser detuning close to the resonant PA transition with the $J = 0$ and $J = 2$ rotational levels of the excited Cs molecule in the $v = 10$ vibrational level, where PA laser wave number is about 11 672.039 $\mathrm{cm^{-1}}$ for the resonant transition to the $J = 0$ rotational level. In each case, we have observed a maximum loss of atoms for a magnetic field close to the resonance position, as can be expected from the Feshbach-optimized PA [30,31]. However, both spectra of atom loss for $J = 0$ and $J = 2$ feature asymmetric variations with respect to the magnetic field, which is particularly pronounced for $J = 0$, where two distinctive peaks manifestly show up. These observations cannot be explained by the theory of enhancing PA using Feshbach resonance [32,33]; instead, they represent a clear manifestation of the Fano effect, as we will soon explain.

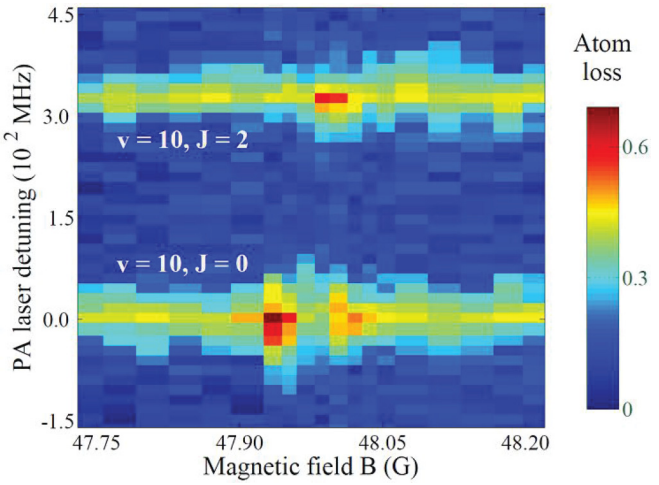

FIG. 2. Two-dimensional spectra of atom-loss strength. The number of atoms remaining in the trap after PA is recorded as a function of PA laser frequency at different B around the d-wave Feshbach resonance. The color map is inverted to show that the PA-induced trap loss increases with a shift from blue to red.

By keeping the laser far off the PA resonance, we find that the atom loss induced solely by the magnetic field is so small that it can be ignored. This can be attributed to both the diluteness of the atomic gas at thermal equilibrium and the narrowness of the d-wave Feshbach resonance considered here.

To further reveal the Fano effect, we present in Fig. 3 the thermally averaged loss rate of Cs atoms, labeled $K_{\rm av}$, as a function of the magnetic field B, keeping the laser frequency ω_L fixed on near resonance. Here $K_{\rm av}$ is determined from the time evolution of the atomic density $\dot{n}(t) = -K_{\rm av} n^2(t)$ [34]. The errors are mainly from the systematic uncertainty induced by the fluctuation of the number of optically trapped atoms in each experimental cycle, the error in determining the resonance frequency of the PA laser, and the controlling precision of the magnetic field near the Feshbach resonance. For the rotational level $J = 0$ of the excited Cs molecule, we have taken two different vibrational levels [$v = 10$ and $v = 17$; see Figs. 3(a) and 3(b), respectively], and for $J = 2$, we have chosen $v = 10$ [see Fig. 3(c)]. Similar to the previously observed coupled dual Fano profiles [28], the key features of Figs. 3(a)–3(c) are the presence of two peaks reflecting the existence of dual Fano profiles, with one having a stronger asymmetric line shape than the other. In addition, we see that different choices of excited molecular levels, in particular the rotational level J, can significantly affect the Fano shape.

We now provide a theory for the above atom loss spectra in terms of the dual Fano resonances, as illustrated in Fig. 1(c). The Hamiltonian involving the scattering state of atoms in the continuum, the bound d-wave Feshbach molecular state, two excited molecular states, and the artificial channel is given by $H = H_0 + H_I$, where the noninteracting Hamiltonian H_0 is expressed as

$$H_0 = \int E dE \sum_{\ell, m_\ell} | E, \ell m_\ell \rangle\langle E, \ell m_\ell | - \sum_{n=1,2} \hbar\delta_n | b_n \rangle\langle b_n | + E_c | b_c \rangle\langle b_c | + \int E'' dE'' | E'' \rangle_{\rm art\ art}\langle E'' | . \quad (1)$$

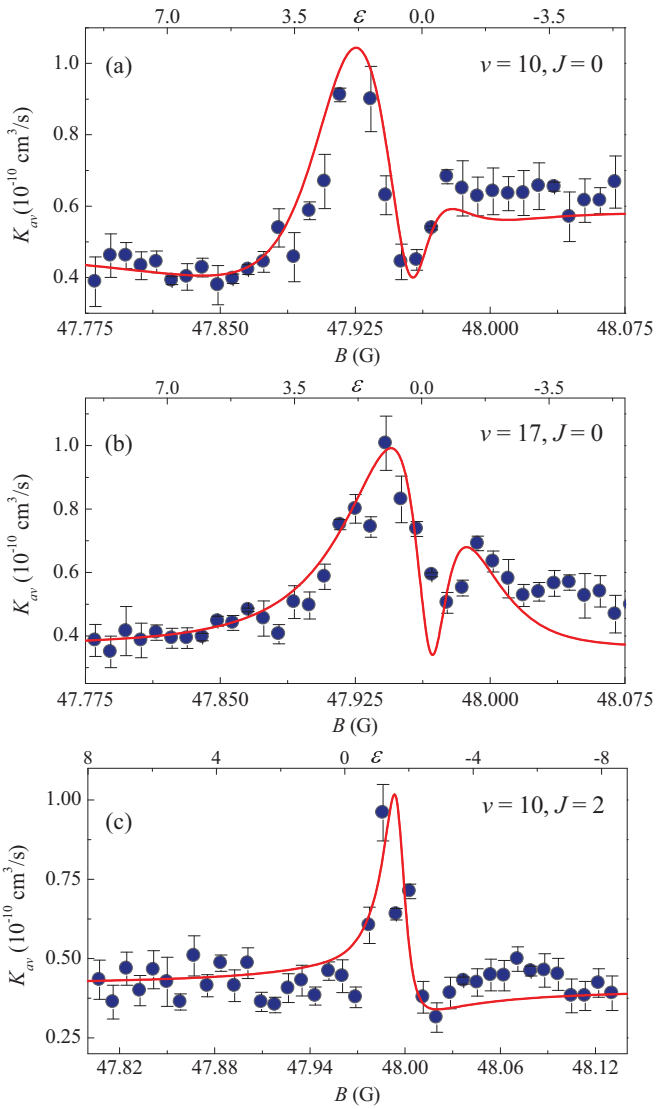

FIG. 3. $K_{\rm av}$ (spheres with error bars) as a function of B near the d-wave Feshbach resonance for the rovibrational levels (a) $v = 10, J = 0$, (b) $v = 17, J = 0$, and (c) $v = 10, J = 2$. By combining the observed Fano minimum in B with other chosen parameters, we have (a) $q_1 = -0.3$ and $q_2 = 21.69$, (b) $q_1 = 0.3$ and $q_2 = 21.69$, and (c) $q_1 = 3.37$ and $q_2 = 7.82$. The solid line shows the prediction of the analytical theory from the coupled dual Fano resonances model with (a) $\Gamma_1 = 15.5$ MHz and $\Gamma_2 = 0.04$ MHz, (b) $\Gamma_1 = 10.5$ MHz and $\Gamma_2 = 0.001$ MHz, and (c) $\Gamma_1 = 6.2$ MHz and $\Gamma_2 = 0.3$ MHz.

Hamiltonian H_I describes the coupling, i.e.,

$$H_I = \sum_{\ell m_\ell} \int dE V_E^{\ell m_\ell} | b_c \rangle\langle E, \ell m_\ell | + \sum_{n=1,2} \Omega_n | b_c \rangle\langle b_n | + \sum_n \sum_{\ell m_\ell} \int dE \Lambda_n^{\ell m_\ell}(E) | b_n \rangle\langle E, \ell m_\ell | + \sum_n \int dE'' V_{n,\rm art}(E'') | b_n \rangle_{\rm art}\langle E'' | + {\rm c.c.} \quad (2)$$

Let $\vec{\ell}$ be the rotational angular momentum of relative motion of the two atoms and m_ℓ be its projection along the

space-fixed z axis. States $|b_c\rangle$ and $|E, \ell m_\ell\rangle$ are connected by Feshbach coupling V that arises from the second-order spin-orbit and spin-spin dipole interactions [35], with the matrix element being $V_E^{\ell m_\ell} = \langle b_c|V|E, \ell m_\ell\rangle$. The free-bound coupling between $|E, \ell m_\ell\rangle$ and $|b_{1(2)}\rangle$ is represented by $\Lambda_{1(2)}^{\ell m_\ell}$, which is responsible for the PA stimulated linewidth $\Gamma_{1(2)}$. The optical transition process between $|b_c\rangle$ and $|b_{1(2)}\rangle$ is described by the Rabi frequency $\Omega_{1(2)}$. Following Fano theory, we can derive the dressed continuum state $|E, \hat{k}\rangle$, which is a coherent superposition of $|b_1\rangle$, $|b_2\rangle$, $|b_c\rangle$, $|E\rangle$, and $|E''\rangle_{\rm art}$. It is mainly the spontaneous decay from such a dressed continuum $|E, \hat{k}\rangle$ or, effectively, from a coherent superposition of $|b_1\rangle$ and $|b_2\rangle$ that leads to the loss of atoms from the trap, as shown in Figs. 2 and 3. Our analytical results of $K_{\rm av}$ (see the detailed derivation in the Appendix) show good agreement with the experimental data.

IV. THEORETICAL METHODS

To understand the different asymmetric Fano lines and the different amplitudes of two peaks exhibited by various rovibrational molecular levels in Fig. 3, we use the microscopic expressions of the Fano parameter q_n contained in the analytical expression of the probability amplitude for excitation of $|b_n\rangle$ $(n = 1, 2)$ in the dressed continuum $|E, \hat{k}\rangle$ (see the Appendix and Ref. [22]). This is given by ($\hbar = 1$)

$$q_n = \frac{\Omega_n + V_{n,\rm eff}}{\pi \sum_{\ell m_\ell} \Lambda_n^{\ell m_\ell} V_E^{\ell m_\ell}}, \tag{3}$$

where $n = 1, 2$ and $V_{n,\rm eff}(E) = \sum_{\ell, m_\ell} P \int dE' \frac{V_{E'}^{\ell m_\ell} \Lambda_{\ell m_\ell}^n(E')}{E - E'}$ is the effective coupling between $|b_c\rangle$ and $|b_n\rangle$ mediated through the continuum. Since the different choices of v are shown to have little influence on the Fano asymmetry parameter, the ratio Ω_n/Γ_n is mostly insensitive to the vibrational level v for the same J, as we see in Figs. 3(a) and 3(b). By contrast, for the same vibrational level $v = 10$, the selection rules allow for a much stronger bound-bound coupling, and thus a larger Ω, for the rotational level $J = 2$ than for $J = 0$. This implies that, according to Eq. (3), the Fano parameter q can change significantly for different rotational levels J. Indeed, comparisons of Figs. 3(a) and 3(c) reveal a much larger q_1 for $J = 2$ than $J = 0$. We note that, for $J = 2$, Γ_2 and therefore $\Lambda_2^{\ell m_\ell}$ are also enhanced compared to the $J = 0$ counterparts. Thus, a reduced q_2 in Fig. 3(c) can be understood to be a consequence of the trade-off between the increases in both Ω_2 and Γ_2. We moreover see that the linewidth determined from the loss rate in Fig. 3(c) is very close to the narrow linewidth Γ_f of the d-wave Feshbach resonance. This can be attributed to the dominant bound-bound transitions in the Fano resonances observed in our case. All plots in Fig. 3 feature the existence of a small peak, corresponding to the second Fano maximum, on the right side of the first dominant Fano minimum, which results from $\Gamma_2 < \Gamma_1$. We remark that all parameters Γ are smaller than the linewidth of the spontaneous decay γ, as required by the unitarity-limited PA [29].

V. CONCLUSION

In summary, we have demonstrated the Fano effect in an ultracold atom-molecule coupled system, where the PA-induced transitions from both the atomic continuum and quasibound molecular state to the excited molecular state form quantum interferences. A theoretical model of dual Fano resonances shows good agreement with our experimental results. In a broader context, our findings will offer insights into the fundamental aspect of the interference of resonances as a key mechanism for the creation of bound states in the continuum in an ultracold atom-molecular system [36,37].

ACKNOWLEDGMENTS

We thank Profs. P. Zhang and Y. Hu for useful comments and discussions. This work was supported by the National Key Research and Development Program of China (Grant No. 2017YFA0304203), the Changjiang Scholars and Innovative Research Team in University of the Ministry of Education of China (Grant No. IRT13076), the National Natural Science Foundation of China (Grants No. 61722507, No. 61675121, No. 61705123, and No. 11434007).

APPENDIX: DERIVATION OF THE PHOTOASSOCIATION RATE

In the presence of a magnetic Feshbach resonance, we use a photoassociation (PA) laser tuned near the rotational level $J = 0$ or $J = 2$ of the vibrational state $v = 10$ or $v = 17$ in the excited molecular 0_g^- potential for Cs_2 below the $(6S_{1/2} + 6P_{3/2})$ dissociation. Here the rotational angular momentum is defined by $\mathbf{J} = \mathbf{L} + \mathbf{S} + \vec{\ell}$, where $\mathbf{L}$ and $\mathbf{S}$ represent the molecular electronic orbital and spin angular momenta and $\vec{\ell}$ is the rotational angular momentum of the relative motion of the two atoms that constitute the molecule. In our theoretical modeling, we consider hyperfine interaction in both the ground- and excited-state potentials. Then the total angular momentum is $\vec{\mathcal{T}} = \mathbf{f} + \vec{\ell} = \mathbf{J} + \mathbf{I}$, where $\mathbf{f} = \mathbf{F}_a + \mathbf{F}_b = \mathbf{J}_e + \mathbf{I}$, $\mathbf{F}_{a(b)}$ is the hyperfine angular momentum of atom a (b), $\mathbf{J}_e = \mathbf{L} + \mathbf{S}$ is the total electronic angular momentum, and $\mathbf{I}$ is the total nuclear spin of the two atoms. In the presence of an external magnetic field B, $\mathcal{T}$ is not a good quantum number; however, its projection $M = m_f + m_\ell$ on the z axis remains a good quantum number. Nevertheless, at a low magnetic field, f and m_f can be considered approximately as conserved quantities.

Here we use a simplified model with multiple bound states coupled to a continuum within the framework of Fano's theory [3]. Our model uses two ground-state channels: one of the channels is open, and the other is closed. We assume that the low-energy scattering under the influence of an external magnetic fields exhibits a d-wave magnetic Feshbach resonance (MFR), which was studied previously by the groups of Chu and Grimm [25,38]. In our two-channel modeling of this Feshbach resonance, the open channel is asymptotically characterized by $|(F_a = 3, F_b = 3)f = 6, \ell = 0; m_f = 6\rangle$, and the closed channel corresponds to $|(F_a = 3, F_b = 3)f = 4, \ell = 2; m_f = 4\rangle$ in the absence of a magnetic field. The channel $|c\rangle$ supports a bound state $|b_c\rangle$. Due to the hyperfine splitting of the excited molecular state, we assume that a single PA laser can couple several excited bound molecular states. For simplicity, we consider two excited bound states, $|b_1\rangle \equiv$

$|(v,J)f_1, m_{f1}\rangle$ and $|b_2\rangle \equiv |(v,J)f_2, m_{f2}\rangle$, coupled to the $|E\rangle$ and $|b_c\rangle$ states.

Using the partial wave decomposition, the open channel bare scattering state $|E\rangle$ in the absence of any external field can be expressed as a superposition of partial-wave scattering states $|E, \ell m_\ell\rangle$. The state $|E, \ell m_\ell\rangle$ is coupled to $|b_c\rangle$ by the second-order spin-orbit and spin-spin dipole interactions [35]. To include spontaneous emission phenomenologically in our model, we assume that both $|b_1\rangle$ and $|b_2\rangle$ decay to the same artificial channel $|E''\rangle_{\rm art}$ as first introduced by Bohn and Julienne [29]. Let the interaction of an excited bound state with $|E''\rangle_{\rm art}$ be $V_{\rm art}$. The relationship of the known spontaneous emission linewidth γ_n with $V_{\rm art}$ is given by $\hbar\gamma_n = 2\pi|_{\rm art}\langle E'' \mid V_{\rm art} \mid b_n\rangle|^2$. The loss of atoms due to this spontaneous emission at a particular collision energy E is described by the loss rate $K_E(\omega_L, B)$.

To calculate the analytic loss rate of atoms we need to diagonalize the Hamiltonian H given in the main text following Fano's method [3] and obtain the probability amplitude of excited states $|b_n\rangle$ for the T matrix. The coupling V_E^{ℓ,m_ℓ} related to the Feshbach resonance line width $\Gamma_f = 2\pi\sum_{\ell,m_\ell}|V_E^{\ell,m_\ell}|^2$ is a function of the collision energy E. Since the Feshbach resonance occurs at a very low energy (<5 μK) almost close to the threshold, we expect $\Gamma_f(E)$ to have a maximum at the energy $E \neq 0$ since in the limit $E \to 0$ we have $V_E \to 0$. Similarly, the other two free-bound PA stimulated linewidths Γ_1 and Γ_2 are also energy dependent. In fitting our model to the experimental data, we have assumed that Γ_f, Γ_1, and Γ_2 are weakly energy dependent near the energy where the Feshbach coupling is the maximum. Another important parameter of our model is the spontaneous linewidth, which we fix at $\gamma_1 = \gamma_2 = \gamma_{sp} \simeq 17$ MHz [39]. For our numerical illustration, we have set $\Gamma_f = 0.065$ MHz [21].

The diagonalization of the model Hamiltonian yields the dressed continuum state

$$
\begin{aligned}
|E,\hat{k}\rangle = \sum_{\ell' m_{\ell'}} Y^*_{\ell' m_{\ell'}}(\hat{k})\Bigg[& \sum_n A_n^{\ell' m_{\ell'}}(E)\mid b_n\rangle + B_E^{\ell' m_{\ell'}}\mid b_c\rangle \\
& + \sum_{\ell m_\ell}\int dE' C^{\ell' m_{\ell'}}_{E',\ell m_\ell}\mid E',\ell m_\ell\rangle \\
& + \int dE'' D^{\ell' m_{\ell'}}_{E''}\mid E''\rangle_{\rm art}\Bigg],
\end{aligned}
\tag{A1}
$$

where $\hat{k}$ is a unit vector along the incident relative momentum of the two atoms and $B_E^{\ell' m_{\ell'}}$, $A_n^{\ell' m_{\ell'}}$, $C^{\ell' m_{\ell'}}_{E',\ell m_\ell}$, and $D^{\ell' m_{\ell'}}_{E''}$ are the expansion coefficients.

We briefly discuss here the method of the derivation of the dressed continuum of Eq. (A1). In particular, we can obtain an analytical expression of the coefficient $A_n^{\ell' m_{\ell'}}$, which is the probability amplitude for excitation of $\mid b_n\rangle$ $(n = 1, 2)$ when the incident partial wave of the relative motion of the two atoms is ℓ' and its projection along the space-fixed z axis is $m_{\ell'}$. From the time-independent Schrödinger equation $\hat{H}|E,\hat{k}\rangle = E|E,\hat{k}\rangle$, we obtain a set of five coupled algebraic equations for $A_1^{\ell' m_{\ell'}}$, $A_2^{\ell' m_{\ell'}}$, $B_E^{\ell' m_{\ell'}}$, $D_{E''}^{\ell' m_{\ell'}}$, and $C^{\ell' m_{\ell'}}_{E'\ell m_\ell}(E)$. The partial-wave symbols appearing in the superscript and subscript of $C^{\ell' m_{\ell'}}_{E'\ell m_\ell}$ refer to the incident and scattered partial waves, respectively. $C^{\ell' m_{\ell'}}_{E'\ell m_\ell}$ is required to fulfill the scattering boundary conditions at a large separation of the two atoms. We first eliminate $C^{\ell' m_{\ell'}}_{E'\ell m_\ell}$ and $D_{E''}^{\ell' m_{\ell'}}$ to obtain three coupled equations for the amplitudes of the three bound states of our model. We can then explicitly solve these three coupled equations. We introduce the dimensionless energy parameter $\epsilon = (E - E_c - E_c^{\rm shift})/(\Gamma_f/2)$, where $E_c^{\rm shift}$ is the shift of $|b_c\rangle$ due to the interchannel coupling, and express $A_n^{\ell' m_{\ell'}}(E)$ in the form

$$
A_n^{\ell' m_{\ell'}} = \mathscr{D}_n^{-1}\left[R_n^{\ell' m_{\ell'}} + \xi_{n'}^{-1} Q_{nn'} R_{n'}^{\ell' m_{\ell'}}\right], \quad n \neq n', \tag{A2}
$$

where

$$
R_n^{\ell' m_{\ell'}} = \Lambda_n^{\ell' m_{\ell'}}(E) + (q_n - i)\pi\sum_{\ell m_\ell}\Lambda_n^{\ell m_\ell} V_E^{\ell m_\ell}\frac{V_E^{\ell' m_{\ell'}}}{\frac{\Gamma_f}{2}(\epsilon + i)}, \tag{A3}
$$

$\Lambda_n^{\ell m_\ell}(E)$ is the free-bound coupling between $|b_n\rangle$ and the scattering state $|E, \ell m_\ell\rangle$, and $V_E^{\ell m_\ell}$ is the coupling between $|E, \ell m_\ell\rangle$ and $|b_c\rangle$ due to the second-order spin-orbit and spin-spin dipole interactions. The stimulated linewidth of PA is $\Gamma_n = 2\pi\sum_{\ell m_\ell}|\Lambda_n^{\ell m_\ell}|^2$. The Fano q parameter q_n is defined by

$$
q_n = \frac{\Omega_n + V_{n,\rm eff}}{\pi\sum_{\ell m_\ell}\Lambda_n^{\ell m_\ell} V_E^{\ell m_\ell}}, \tag{A4}
$$

where

$$
V_{n,\rm eff}(E) = \sum_{\ell m_\ell}\mathcal{P}\int dE' \frac{V_{E'}^{\ell m_\ell}\Lambda^n_{\ell m_\ell}(E')}{E - E'} \tag{A5}
$$

is the effective coupling between $|b_c\rangle$ and $|b_n\rangle$ mediated through the open-channel continuum. Here $\mathcal{P}$ implies the principal value integral. Here

$$
\begin{aligned}
\mathscr{D}_n = {} & E + \hbar\delta_n - E_{n,\rm pa}^{\rm shift} - E_{qn}^{\rm shift} + i\hbar(\gamma_n + \Gamma_{qn})/2 \\
& - \xi_{n'}^{-1} Q_{nn'} Q_{n'n},
\end{aligned}
\tag{A6}
$$

with $\Gamma_{qn} = \Gamma_n - 2{\rm Im}\mathscr{E}_{qn}$ and $E_{qn}^{\rm shift} = {\rm Re}\mathscr{E}_{qn}$, where

$$
\mathscr{E}_{qn} = \frac{\left[(q_n - i)\pi\sum_{\ell m_\ell}\Lambda_n^{\ell m_\ell} V_E^{\ell m_\ell}\right]^2}{\frac{\Gamma_f}{2}(\epsilon + i)}. \tag{A7}
$$

The PA laser-intensity-induced shift of $|b_n\rangle$ in the absence of magnetic field is $E_{n,\rm pa}^{\rm shift} = \sum_{\ell m_\ell}\mathcal{P}\int dE' \frac{|\Lambda_n^{\ell m_\ell}(E')|^2}{E - E'}$. The term $Q_{nn'}$ can be expressed by

$$
\begin{aligned}
Q_{nn'} = {} & \sum_{\ell m_\ell}\int dE' \frac{\Lambda_n^{\ell m_\ell}(E')\{\Lambda_{n'}^{\ell m_\ell}(E')\}^*}{E - E'} \\
& + \left((q_n - i)\pi\sum_{\ell m_\ell}\Lambda_n^{\ell m_\ell} V_E^{\ell m_\ell}\right) \\
& \times \frac{\pi\sum_{\ell m_\ell}\Lambda_{n'}^{\ell m_\ell} V_E^{\ell m_\ell}(q_{n'} - i)}{\frac{\Gamma_f}{2}(\epsilon + i)}.
\end{aligned}
\tag{A8}
$$

The first term on the right-hand side of Eq. (A8) arises due to the laser-induced coupling, and the second is caused by the combined effect of laser and magnetic fields. As a

result of these couplings, the spontaneous emissions from the two excited bound states become correlated. Thus, it is the spontaneous decay from the dressed continuum or, effectively, from a coherent superposition state of the two bound states that leads to the loss of the atoms from the trap. The overall shift of the state $|b_n\rangle$ in the presence of magnetic field is then given by

$$E_{\rm shift} = E^{\rm shift}_{n,\rm pa} + E^{\rm shift}_{qn} + {\rm Re}\big[\xi^{-1}_{n'} Q_{nn'} Q_{n'n}\big]. \tag{A9}$$

The T-matrix element for transition to the artificial decay channel is given by

$$T_{\rm decay} = {}_{\rm art}\langle E'' \mid V_{\rm art} \mid E, \hat{k}\rangle = \sum_n V_{n,\rm art} A^{\ell' m_{\ell'}}_n. \tag{A10}$$

Since the s-wave contribution is most significant near the threshold, if we neglect the term $Q_{nn'}$, we can use $V^{00}_E \simeq \sqrt{\Gamma_f/(2\pi)}$ and $\Lambda^{00}_n \simeq \sqrt{\Gamma_n/(2\pi)}$. Then R^{00}_n of Eq. (A3) reduces to the standard Fano profile form $F_n = \frac{\epsilon+q_n}{\epsilon+i}$. Clearly, $T_{\rm decay}$ reduces to a superposition of two Fano profiles. As shown in Ref. [28] of the main text, we have found that our results are strongly affected by the term $Q_{nn'}$ and thus deviate from the standard Fano profile. The S-matrix element for the decay is given by

$$S_{\rm decay} = -2\pi i T_{\rm decay}. \tag{A11}$$

The total inelastic scattering rate due to spontaneous emission is given by

$$\sigma_{\rm inel} = \frac{\pi}{k^2} \mid S_{\rm decay} \mid^2 . \tag{A12}$$

The unitarity limit dictates that $\mid S_{\rm decay} \mid^2 \leqslant 1$. The loss rate at energy E is given by

$$K_E(\omega_L, B) = v_{\rm rel}\sigma_{\rm inel}, \tag{A13}$$

where $v_{\rm rel}$ is the relative velocity related to the collision energy, which is given by $E = \mu v^2_{\rm rel}/2 = \hbar^2 k^2/2\mu$. In fact, the observed loss rate has a narrow line, which means that only the low-energy atoms ($E < 3.5 k_B\ \mu$K) contribute to the Fano effect. We thus have the thermally averaged loss rate at the temperature T near the Feshbach resonance,

$$K_{\rm av}(\omega_{\rm L}, B) = \frac{4\pi^2\hbar^2}{(2\pi\mu k_B T)^{3/2}} \times \int dE \exp\left(-\frac{E}{k_B T}\right) |S_{\rm decay}|^2. \tag{A14}$$

At low collision energy E, close to the threshold of the open channel, $|S_{\rm decay}|^2$ is a slowly varying function of E.

Since the closed-channel bound-state energy is approximately a linearly varying function of B near the resonant value B_0, we expect that the derived formula will give accurate results only near B_0. According to the above formula, we plot $K_{\rm av}$ as a function of B for the fixed laser detuning δ_n. The fitting parameters are given in the caption of Fig. 3 in the main text, and the input parameters are chosen based on the earlier works on the d-wave Feshbach resonance of Cs atoms in the hyperfine state $F = 3$, $m_F = 3$ [25,38]. For a good fitting of the experimental data, we add a small off-resonant background contribution in $K_{\rm av}$. As shown in Fig. 3 in the main text, the theoretical result shows good agreement with experimental data. Here $K_{\rm av}$ is given by the absolute square of the superposition of two Fano profiles; it is consistent with the fact that the spectra exhibit two peaks and one or two minima. No peak exceeds the unitarity limit $S_{\rm decay} \to 1$. Note that the free-bound and bound-bound PA transitions predominantly occur at interatom separations of around $20a_0$, where a_0 is the Bohr radius. At such a separation, several asymptotic channels can be mixed up by spin-orbit, spin-spin dipole, and hyperfine interactions. In fact, earlier calculations [25] for MFR show that one has to take into account at least 24 channels in order to get accurate quantitative results. Therefore, our model, which uses only two ground-state channels and two excited bound states, is a simplified version of the actual physical situation. Nevertheless, we get reasonable agreement between theory and experiment.

[1] M. Flesichhauer, A. Imamolu, and J. P. Marangos, Electromagnetically induced transparency: Optics in coherent media, Rev. Mod. Phys. **77**, 633 (2005).

[2] A. E. Miroshnichenko, S. Flach, and Y. S. Kivshar, Fano resonances in nanoscale structures, Rev. Mod. Phys. **82**, 2257 (2010).

[3] U. Fano, Effects of configuration interaction on intensities and phase shifts, Phys. Rev. **124**, 1866 (1961).

[4] A. R. P. Rau, Perspectives on the Fano Resonance Formula, Phys. Scr. **69**, C10 (2004).

[5] S. H. Linn, W.-B. Tzeng, J. M. Brom, Jr., and C. Y. Ng, Molecular beam photoionization study of $HgBr_2$ and HgI_2, J. Chem. Phys. **78**, 50 (1983).

[6] R. P. Madden and K. Codling, New Autoionizing Atomic Energy Levels in He, Ne, and Ar, Phys. Rev. Lett. **10**, 516 (1963).

[7] U. Fano and J. W. Cooper, Spectral distribution of atomic oscillator strengths, Rev. Mod. Phys. **40**, 441 (1968).

[8] H. Feshbanch, Unified theory of nuclear reactions, Ann. Phys. (N.Y.) **5**, 357 (1958).

[9] H. Feshbanch, A unified theory of nuclear rections. II, Ann. Phys. (N.Y.) **19**, 287 (1962).

[10] A. R. Schmidt, M. H. Hamidian, P. Wahl, F. Meier, A. V. Balatsky, J. D. Garrett, T. J. Williams, G. M. Luke, and J. C. Davis, Imaging the Fano lattice to 'hidden order' transition in URu_2Si_2, Nature (London) **465**, 570 (2010).

[11] J. A. Fan, C. Wu, K. Bao, J. Bao, R. Bardhan, N. J. Halas, V. N. Manoharan, P. Nordlander, G. Shvets, and F. Capasso, Self-assembled plasmonic nanoparticle clusters, Science **328**, 1135 (2010).

[12] J. D. Lee, J. Inoue, and M. Hase, Ultrafast Fano Resonance Between Optical Phonons and Electron-Hole Pairs at the Onset of Quasiparticle Generation in a Semiconductor, Phys. Rev. Lett. **97**, 157405 (2006).

[13] M. Kroner, A. O. Govorov, S. Remi, B. Biedermann, S. Seidl, A. Badolato, P. M. Petroff, W. Zhang, R. Barbour, B. D. Gerardot, R. J. Warburton, and K. Karrai, The nonlinear Fano effect, Nature (London) **451**, 311 (2008).

[14] Y. B. Zhang, X. Y. Hu, Y. L. Fu, H. Yang, and Q. H. Gong, Ultrafast all-optical tunable Fano resonance in nonlinear ferroelectric photonic crystals, Appl. Phys. Lett. **100**, 031106 (2012).

[15] N. Liu, L. Langguth, T. Weiss, J. Kästel, M. Fleischhauer, T. Pfau, and H. Giessen, Plasmonic analog of electromagnetically induced transparency at the Drude damping limit, Nat. Mater. **8**, 758 (2009).

[16] C. Chen, I. Un, N. Tai, and T. Yen, Asymmetric coupling between subradiant and superradiant plasmonic resonances and its enhanced sensing performance, Opt. Express **17**, 15372 (2009).

[17] Z. Chai, X. Y. Hu, and Q. H. Gong, All-optical switching based on a tunable Fano-like resonance in nonlinear ferroelectric photonic crystals, J. Opt. **15**, 085001 (2013).

[18] F. Neubrech, A. Pucci, T. W. Cornelius, S. Karim, A. García-Etxarri, and J. Aizpurua, Resonant Plasmonic and Vibrational Coupling in a Tailored Nanoantenna for Infrared Detection, Phys. Rev. Lett. **101**, 157403 (2008).

[19] E. J. Osley, C. G. Biris, P. G. Thompson, R. R. F. Jahromi, P. A. Warburton, and N. C. Panoiu, Fano Resonance Resulting from a Tunable Interaction between Molecular Vibrational Modes and a Double Continuum of a Plasmonic Metamolecule, Phys. Rev. Lett. **110**, 087402 (2013).

[20] L. Stern, M. Grajower, and U. Levy, Fano resonances and all-optical switching in a resonantly coupled plasmonic-atomic system, Nat. Commun. **5**, 4865 (2013).

[21] C. Chin, R. Grimm, P. S. Julienne, and E. Tiesinga, Feshbach resonances in ultracold gases, Rev. Mod. Phys. **82**, 1225 (2010).

[22] B. Deb and G. S. Agarwal, Feshbach resonance-induced Fano interference in photoassociation, J. Phys. B **42**, 215203 (2009).

[23] Y. Q. Li, G. S. Feng, R. D. Xu, X. F. Wang, J. Z. Wu, G. Chen, X. C. Dai, J. Ma, L. T. Xiao, and S. T. Jia, Magnetic levitation for effective loading of cold cesium atoms in a crossed dipole trap, Phys. Rev. A **91**, 053604 (2015).

[24] T. Weber, J. Herbig, M. Mark, H.-C. Nägerl, and R. Grimm, Three-Body Recombination at Large Scattering Lengths in an Ultracold Atomic Gas, Phys. Rev. Lett. **91**, 123201 (2003).

[25] C. Chin, V. Vuletić, A. J. Kerman, S. Chu, E. Tiesinga, P. J. Leo, and C. J. Williams, Precision Feshbach spectroscopy of ultracold Cs_2, Phys. Rev. A **70**, 032701 (2004).

[26] N. Bouloufa, A. Crubellier, and O. Dulieu, Reexamination of the 0_g^- pure long-range state of Cs_2: Prediction of missing levels in the photoassociation spectrum, Phys. Rev. A **75**, 052501 (2007).

[27] J. G. Danzl, M. J. Mark, E. Haller, M. Gustavsson, N. Bouloufa, O. Dulieu, H. Ritsch, R. Hart, and H.-C. Nägerl, Precision molecular spectroscopy for ground state transfer of molecular quantum gases, Faraday Discuss. **142**, 283 (2009).

[28] J. A. Armstrong and J. J. Wynne, Autoionizing State of Sr Studied by the Generation of Tunable Vacuum uv Radiation, Phys. Rev. Lett. **33**, 1183 (1974).

[29] J. L. Bohn and P. S. Julienne, Semianalytic theory of laser-assisted resonant cold collisions, Phys. Rev. A **60**, 414 (1999).

[30] B. L. Tolra, N. Hoang, B. T'Jampens, N. Vanhaecke, C. Drag, A. Crubellier, D. Comparat, and P. Pillet, Controlling the formation of cold molecules via a Feshbach resonance, Europhys. Lett. **64**, 171 (2003).

[31] M. Junker, D. Dries, C. Welford, J. Hitchcock, Y. P. Chen, and R. G. Hulet, Photoassociation of a Bose-Einstein Condensate near a Feshbach Resonance, Phys. Rev. Lett. **101**, 060406 (2008).

[32] M. Mackie, M. Fenty, D. Savage, and J. Kesselman, Cross-Molecular Coupling in Combined Photoassociation and Feshbach Resonances, Phys. Rev. Lett. **101**, 040401 (2008).

[33] P. Pellegrini, M. Gacesa, and R. Côté, Giant Formation Rates of Ultracold Molecules via Feshbach-Optimized Photoassociation, Phys. Rev. Lett. **101**, 053201 (2008).

[34] C. McKenzie, J. H. Denchlag, H. Häffner, A. Browaeys, L. E. E. de Araujo, F. K. Fatemi, K. M. Jones, J. E. Simsarian, D. Cho, A. Simoni, E. Tiesinga, P. S. Julienne, K. Helmerson, P. D. Lett, S. L. Rolston, and W. D. Phillips, Photoassociation of Sodium in a Bose-Einstein Condensate, Phys. Rev. Lett. **88**, 120403 (2002).

[35] F. H. Mies, C. J. Williams, P. S. Julienne, and M. Krauss, Estimating bounds on collisional relaxation rates of spin-polarized ^{87}Rb atoms at ultracold temperatures, J. Res. Natl. Inst. Stand. Technol. **101**, 521 (1996).

[36] B. Deb and G. S. Agarwal, Creation and manipulation of bound states in the continuum with lasers: Applications to cold atoms and molecules, Phys. Rev. A **90**, 063417 (2014).

[37] A. Kodigala, T. Lepetit, Q. Gu, B. Bahari, Y. Fainman, and B. Kanté, Lasing action from photonic bound states in continuum, Nature (London) **541**, 196 (2017).

[38] M. Mark, F. Ferlaino, S. Knoop, J. G. Danzl, T. Kraemer, C. Chin, H.-C. Nägerl, and R. Grimm, Spectroscopy of ultracold trapped cesium Feshbach molecules, Phys. Rev. A **76**, 042514 (2007).

[39] S. D. Kraft, M. Mudrich, M. U. Staudt, J. Lange, O. Dulieu, R. Wester, and M. Weidemüller, Saturation of Cs_2 photoassociation in an optical dipole trap, Phys. Rev. A **71**, 013417 (2005).